COMSOL CONFERENCE 2024 FLORENCE

Simulation framework for hole spin qubits

Lorenzo Raschi[1], Antonio Gnudi[2]
1. ARCES/DEI, University of Bologna, Bologna, Italy.

Abstract
In the present paper a framework for simulating hole spin qubits using COMSOL Multiphysics is presented. The tool solves the coupled Poisson and Schrödinger equations within the four-bands $\mathbf{k} \cdot \mathbf{p}$ Hamiltonian, accounting for the effects of a static magnetic field $\boldsymbol{B}$. The gyromagnetic matrix g and its derivative g' with respect to the gate voltage are obtained from the wavefunctions at zero magnetic field. The g and g' matrices enable the calculation of the Rabi frequency as a function of the magnetic field, considering first-order contributions from both the magnetic field and gate voltage. Results for a qubit hosted in a silicon nanowire produced with SOI technology are presented.

Keywords: Spin-Qubit, Quantum Computing, Quantum-CAD, Luttinger-Kohn Hamiltonian.

Introduction
Among the different technological platforms being explored for building large-scale multi-qubit quantum computers, spin qubits in silicon quantum dots (QDs) stand out as a highly promising option. This is because isotopically purified silicon allows for long spin lifetimes. Additionally, silicon is well-suited for integrating quantum devices with classical electronics [1]. Hole spin qubits are particularly advantageous over electron spin qubits because the hole spin couples more easily to the orbital motion, enabling purely electrical control of the spin [2].
From a modeling perspective, developing a Quantum-CAD (QCAD) framework is highly valuable for supporting device design and exploring new solutions, similar to how TCAD tools are used in nanoelectronics.
In this paper, we describe a QCAD tool based on COMSOL Multiphysics to study hole spin qubits in semiconductor quantum dots. This tool self-consistently calculates both the electrostatic potential and the energy levels of a hole in a quantum dot under the influence of a static magnetic field. Additionally, it computes the gyromagnetic matrix, which fully describes the qubit properties and allows for the calculation of the Rabi frequency as a function of the magnetic field orientation [3].

Simulated devices
Fig. 1 illustrates the geometry of the simulated structure (see caption for details). It is based on SOI (Silicon-on-Insulator) technology, featuring a [110]-oriented silicon nanowire embedded within an SiO_2 layer that hosts the qubit. Three metal gates are used to create a potential well to trap a hole beneath the central gate. The central gate is biased with a voltage V_{CG}, and a radiofrequency (RF) modulation with amplitude V_{ac} is applied to control the qubit state. The lateral gates are held at a fixed zero voltage. A bottom contact, biased at voltage V_{BC}, serves as a substitute for the doped silicon substrate. The entire structure is covered with a passivating SiO_2 layer, which has been removed in the figure for clarity.

The mathematical model
The potential profile in the device is first computed with Poisson equation. The charge in the Si nanowire is very small and can be neglected in practice. Dirichlet boundary conditions are used in the contacts and Neumann conditions for the remaining boundaries.
The four-band **k·p** Luttinger-Kohn (LK) Hamiltonian [4,5] for the valence band is used to compute the hole eigenstates. Full details and equations are provided in Appendix A. This model essentially accounts for the behavior of the heavy-hole (HH) and light-hole (LH) components of the wavefunction. Schrödinger equation in this case is a system of four PDEs in the four unknown components of the wavefunction envelope. Zero wavefunction boundary conditions are applied at the Si/insulator interfaces, (i.e. the wavefunction is not allowed to penetrate into the insulator regions). Zero boundary condition is also applied to the two terminating faces of the nanowire. This is supposed to be a good approximation, since under the lateral gates the wavefunction is small anyhow, due to the longitudinal confinement.
Rabi frequency can be calculated either using the direct method, leading to Eq. (13) in Appendix B, or through the first-order approximation of the g-matrix formalism described in Appendix C, which follows the theory outlined in reference [3]. The g-matrix approach offers the benefit of not requiring the eigenvalue problem to be solved for every magnetic field orientation, as opposed to the direct method.

COMSOL implementation
Poisson equation is solved with the Poisson equation module.

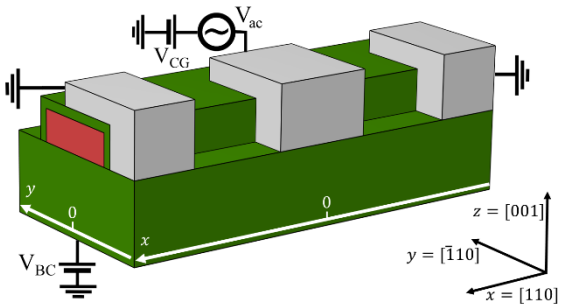

Fig. 1. Simulated structure. Color code: red for Si, green for SiO_2, grey for metal gates. The Si nanowire cross section is 10 nm × 30 nm, the bottom oxide thickness 25 nm, the central gate length 30 nm, the lateral gates length 20 nm, the gate spacing 30 nm, the thin SiO_2 layer thickness 3 nm. The structure is covered by a passivating SiO_2 layer (not shown). The gates overlap 20 nm out of 30 nm of the nanowire. The x axis is parallel to the longitudinal nanowire axis. The crystallographic orientation is illustrated in the inset.

The eigenvalue problem is solved with the Schrödinger equation module. In this case the wavefunction has four components, so the Hamiltonian becomes a 4×4 operator matrix, the elements of which are differential operators of at most second order. These diagonal and off-diagonal elements of the Hamiltonian matrix are entered using built-in features of the Schrödinger Equation physics interface. The benchmark models [6] and [7] from the Application Libraries show how to set up multiple wavefunction components with the Schrödinger Equation interface.

The discretization mesh in the SiO_2 domains consists of free tetrahedral elements, with size ranging from 2.34 nm to 13 nm, built with the "Normal" option. The mesh in the Si domain consists of 4500 (i.e. 15×15×20) finite difference elements; a higher number of elements is chosen in the z-direction, which is the main quantization direction. Fig. 2 shows a discretized section of the structure potential on the cross section at the (y, z) plane.

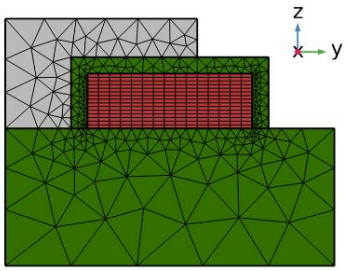

Fig. 2. Example of discretization mesh on a (y, z) plane cross section. The mesh in the SiO_2 domains consists of free tetrahedral elements, built with the "Normal" option. The mesh in the Si domain consists of 15×15×20 finite difference elements.

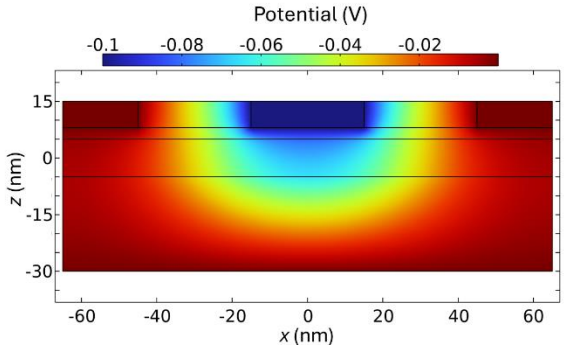

Fig. 3. Electric potential on the cross section at the (x, z) plane at y = 0 (see Fig. 1), for $V_{CG} = -0.1\,V$ and $V_{BC} = 0\,V$.

The calculation of the Rabi frequency requires the computation of elements of the matrix D_1 (Appendix B, Eq. (13)) between the two ground states.

Similarly, the terms of matrices g and g' are computed as elements of the matrix $\boldsymbol{M}_1$(Appendix C, Eq. (16)) involving the zero-field states of the qubit. All such matrix coefficients, involving integrals over the entire Si domain volume, are efficiently calculated by COMSOL with the built-in *intop* function. Finally, LiveLink™ for MATLAB® allows to easily export the computed terms and determine the Rabi frequency (Appendix C, Eq. (17)).

Results

Potential

As an example, electric potential on the cross section at the (x, z) plane at y = 0 is plotted in Fig. 3 for $V_{CG} = -0.1$ V and $V_{BC} = 0$ V, corresponding to one hole captured in the nanowire under the central gate.

Zero field wavefunction

The results presented in this Section are obtained with B = 0 T. At zero magnetic field each energy eigenvalue is double degenerate due to symmetry reasons, forming the so called Kramers doublet. The calculated energy gap between the ground and the first excited doublet at $V_{CG} = -0.1$ V and $V_{BC} = 0$ V is $\Delta E = 4.03$ meV.

The square moduli of the four components of one of the ground states on the (y, z) plane at x = 0 (i.e. just under the central gate, see Fig.1) are reported in Fig. 4. They show a dominant HH (J_z = ±3/2) character.

Rabi frequency

Fig. 5 shows the plot of the Rabi frequency as a function of V_{BC} at $V_{CG} = -0.1$ V, $\boldsymbol{B} = (0,1,1)/\sqrt{2}$ T and $V_{ac} = 1$ mV. The results obtained with the g-matrix formalism (17) are compared with the standard procedure (13). The very good agreement between the two approaches demonstrates that for the applied value of B the device operates in linear regime.

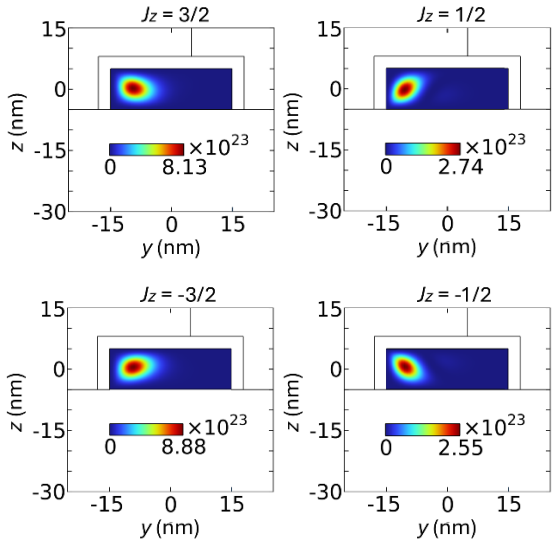

Fig. 4. Squared HH ($J_z = \pm 3/2$) and LH ($J_z = \pm 1/2$) envelopes of the ground-state doublet on the (y, z) plane at x = 0 (see Fig. 1), at V_{CG} = -0.1 V and V_{BC} = 0 V. The HH components are almost four times larger than the LH components.

Conclusions

A simulation framework for hole spin qubits developed using COMSOL Multiphysics is presented, enabling numerical characterization of the device. This tool can serve as a CAD resource for analyzing qubit properties, including sensitivities to geometric parameters, material defects, and process variations. While results have been demonstrated for silicon, the tool is also easily adaptable to other semiconductor materials, such as Ge/SiGe.

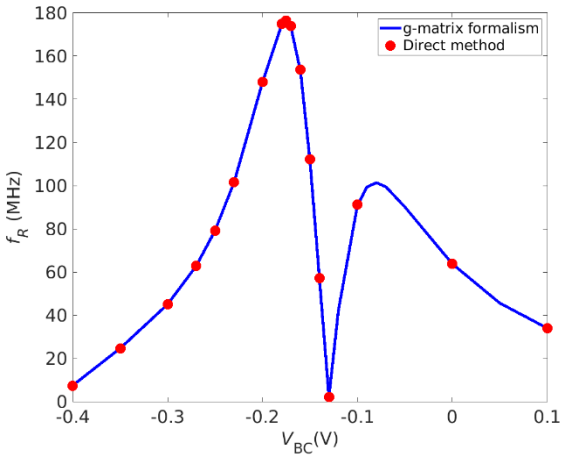

Fig. 5. Rabi frequency vs. V_{BC} for $\boldsymbol{B}$ = (0, 1, 1) /$\sqrt{2}$ T and V_{ac} = 1 mV at V_{CG} = -0.1 V. The results obtained with the g-matrix approach (solid lines) are compared with the standard procedure (circles). The plot shows excellent agreement.

References

[1] G. Burkard, T. D. Ladd, J. M. Nichol, A. Pan, J. R. Petta, Rev. Mod. Phys. 95, 025003 (2023).

[2] Y. Fang, P. Philippopolous, D. Culcer, W A Coish, S. Chesi, Mater. Quantum Technol. 3, 012003 (2023).

[3] B. Venitucci, L. Bourdet, D. Pouzada, Y.-M. Niquet, Phys. Rev. B 98, 155319 (2018).

[4] L. C. Lew Yan Voon and M. Willatzen, *The k·p Method* (Springer, Berlin, 2009).

[5] B. Martinez, J. C. Abadillo-Uriel, E. A. Rodríguez-Mena, Y.-M. Niquet, Phys. Rev. B 106, 235426 (2022).

[6] https://www.comsol.com/model/kp-method-for-strained-wurtzite-gan-band-structure-88271, *k·p Method for Strained Wurtzite GaN Band Structure*.

[7] https://www.comsol.com/model/a-silicon-quantum-dot-in-a-uniform-magnetic-field-88981, *A Silicon Quantum Dot in a Uniform Magnetic Field.*

Appendix A: Hamiltonian model

The hole states are obtained by diagonalizing the four-bands **k** · **p** Luttinger-Kohn (LK) Hamiltonian [4,0] for the valence band. The HH and LH components of the wavefunction are mapped onto the $J_z = \pm\frac{3}{2}$ and $J_z = \pm\frac{1}{2}$ components of a $J = \frac{3}{2}$ total angular momentum, respectively. The total Hamiltonian reads

$$H = H_K + H_Z + V_t(V_{\mathrm{CG}}, \boldsymbol{r}) \tag{1}$$

where H_K is the kinetic term, H_Z the Zeeman term and $V_t(V_{\mathrm{CG}}, \boldsymbol{r})$ the potential energy, which is a function of position and depends on the voltage V_{CG} applied to the central gate. The potential profile is obtained through the solution of Poisson equation.

In the $\left\{\left|\frac{3}{2},\frac{3}{2}\right\rangle, \left|\frac{3}{2},\frac{1}{2}\right\rangle, \left|\frac{3}{2},-\frac{1}{2}\right\rangle, \left|\frac{3}{2},-\frac{3}{2}\right\rangle\right\}$ basis set, the H_K component of the Hamiltonian reads [5]

$$H_K = -\begin{bmatrix} P+Q & -S & R & 0 \\ -S^\dagger & P-Q & 0 & R \\ R^\dagger & 0 & P-Q & S \\ 0 & R^\dagger & S^\dagger & P+Q \end{bmatrix} \tag{2}$$

where

$$P = \frac{\hbar^2}{2m_0}\gamma_1(k_x^2 + k_y^2 + k_y^2) \tag{3}$$

$$Q = \frac{\hbar^2}{2m_0}\gamma_2(k_x^2 + k_y^2 - 2k_z^2) \tag{4}$$

$$R = \frac{\hbar^2}{2m_0}\sqrt{3}\left[-\gamma_3\left(\left(k_x^2 - k_y^2\right) + 2i\gamma_2\{k_x, k_y\}\right]\right. \tag{5}$$

$$S = \frac{\hbar^2}{2m_0}2\sqrt{3}\gamma_3\left[\{k_x - ik_y, k_z\}\right] \tag{6}$$

with $\{A, B\} = \frac{1}{2}(AB + BA)$. Here $\boldsymbol{k} = (k_x, k_y, k_z)$ is the wavevector, m_0 the free electron mass and γ_1, γ_2, γ_3 the Luttinger parameters that characterize the valence band. The reference system axes are defined in Fig. 1. Notice that the *x*-axis, that is the longitudinal nanowire axis, corresponds to the [110] crystal orientation.

At finite magnetic field $\boldsymbol{B}$, the HH and LH components are also mixed by the Zeeman Hamiltonian H_Z

$$H_Z = 2\mu_B(\kappa \boldsymbol{B}\cdot\boldsymbol{J} + q\boldsymbol{B}\cdot\boldsymbol{J}^3) \tag{7}$$

where μ_B is the Bohr magneton, $\boldsymbol{J} = (J_x, J_y, J_z)$ is the spin $\frac{3}{2}$ operator, $\boldsymbol{J}^3 = (J_x^3, J_y^3, J_z^3)$ and κ, q are the isotropic and cubic Zeeman parameters. The $\boldsymbol{J}$ matrices consistent with the basis set of (2) read:

$$J_x = \frac{1}{2}\begin{bmatrix} 0 & \sqrt{3} & 0 & 0 \\ \sqrt{3} & 0 & 2 & 0 \\ 0 & 2 & 0 & \sqrt{3} \\ 0 & 0 & \sqrt{3} & 0 \end{bmatrix} \tag{8}$$

$$J_y = \frac{i}{2}\begin{bmatrix} 0 & -\sqrt{3} & 0 & 0 \\ \sqrt{3} & 0 & -2 & 0 \\ 0 & 2 & 0 & -\sqrt{3} \\ 0 & 0 & \sqrt{3} & 0 \end{bmatrix} \tag{9}$$

$$J_z = \frac{1}{2}\begin{bmatrix} 3 & 0 & 0 & 0 \\ 0 & 1 & 0 & 0 \\ 0 & 0 & -1 & 0 \\ 0 & 0 & 0 & -3 \end{bmatrix}. \tag{10}$$

The action of the magnetic field on the orbital motion of the hole is described by the substitution $\boldsymbol{k} \longrightarrow -i\boldsymbol{\nabla} + e\,\boldsymbol{A}/\hbar$, where $\boldsymbol{A}$ is the vector potential. By choosing the Landau gauge $\nabla\cdot\boldsymbol{A} = \boldsymbol{0}$, for constant magnetic field $\boldsymbol{B}$ the vector potential reads:

$$\boldsymbol{A} = -(yB_z, zB_x, xB_y). \tag{11}$$

It should be noticed that $\boldsymbol{B}$ enters the Hamiltonian through both the Zeeman term H_Z and the kinetic term H_K via the $\boldsymbol{k}$ operator.

Appendix B: direct calculation of the Rabi frequency

This Appendix and the following one closely follow the theory outlined in [3]. Consider a QD in a homogeneous and static magnetic field $\boldsymbol{B}$. Assume the central gate voltage $V_{\mathrm{CG}}(t) = V_0 + V_{\mathrm{ac}}\sin(2\pi f t + \varphi)$, with V_0 the reference bias voltage. The Hamiltonian can then be expressed as

$$H(V_{\mathrm{CG}}, \boldsymbol{B}) = H_0(V_{\mathrm{CG}}) - \boldsymbol{B}\cdot\boldsymbol{M}_1 + \mathcal{O}(B^2) \tag{12}$$

where $\boldsymbol{M}_1 = \left(M_{1,x}\, M_{1,y}\, M_{1,z}\right)$ is a vector composed of three matrices $M_{1,k} = -\left.\frac{\partial H}{\partial B_k}\right|_{\boldsymbol{B}=0}$ and is assumed to be independent of V_{CG}. We label $|\mathbb{1}\rangle, |\mathbb{0}\rangle$ the lowest-energy eigenstates of $H(V_0, \boldsymbol{B})$. The corresponding eigenenergies are $E_{\mathbb{1}}$ and $E_{\mathbb{0}}$, respectively. At $\boldsymbol{B} = \boldsymbol{0}$ the two states are degenerate (Kramers doublet). Degeneracy is broken with the application of the finite static magnetic field: the two eigenenergies are split by the Zeeman energy $\Delta E = E_{\mathbb{1}} - E_{\mathbb{0}} = g^*\mu_B B$, where g^* is the effective gyromagnetic factor that may depend on the orientation of $\boldsymbol{B}$. The RF modulation of the voltage $V_{\mathrm{CG}}(t)$ at resonance ($hf = \Delta E$) produces coherent oscillations between states $|\mathbb{0}\rangle$ and $|\mathbb{1}\rangle$ with Rabi frequency

$$f_R = \frac{e}{h}V_{ac}|\langle\mathbb{1}|D_1|\mathbb{0}\rangle|, \tag{13}$$

where $D_1(\boldsymbol{r}) = \left.\frac{\partial V_t(V_{\mathrm{CG}}, \boldsymbol{r})}{\partial V_{\mathrm{CG}}}\right|_{V_{\mathrm{CG}}=V_0}$ is the derivative of the potential energy $V_t(V_{\mathrm{CG}}, \boldsymbol{r})$ with respect to the gate voltage V_{CG}.

Appendix C: Rabi frequency in the *g*-matrix formalism

Recalling the $H(V_{\mathrm{CG}}, \boldsymbol{B})$ expression (12), we can also expand the $\boldsymbol{B}$-independent term $H_0(V_{\mathrm{CG}})$ in powers of $\delta V = V_{\mathrm{CG}} - V_0$

$$H_0(V_{\mathrm{CG}}) = H_0(V_0) + (\delta V)D_1 + \mathcal{O}(\delta V^2), \quad (14)$$

and we call $|\Uparrow\rangle, |\Downarrow\rangle$ the degenerate Kramers doublet eigenstates of $H_0(V_0)$. To first order in $\boldsymbol{B}$ and V_{ac}, an effective two-states Hamiltonian can be derived having the form

$$H_{\mathrm{eff}}(V_{\mathrm{CG}}, \boldsymbol{B}) = \frac{1}{2}\mu_B\, \boldsymbol{\sigma} \cdot g(V_{\mathrm{CG}})\boldsymbol{B}, \quad (15)$$

where $\boldsymbol{\sigma}$ is the vector formed of the Pauli matrices and g is a real 3×3 matrix called gyromagnetic matrix. For $V_{\mathrm{CG}} = V_0$ the g-matrix can be expressed as

$$g(V_0) = -\frac{2}{\mu_B}\begin{bmatrix} Re\langle\Downarrow|M_{1,x}|\Uparrow\rangle & Re\langle\Downarrow|M_{1,y}|\Uparrow\rangle & Re\langle\Downarrow|M_{1,z}|\Uparrow\rangle \\ Im\langle\Downarrow|M_{1,x}|\Uparrow\rangle & Im\langle\Downarrow|M_{1,y}|\Uparrow\rangle & Im\langle\Downarrow|M_{1,z}|\Uparrow\rangle \\ \langle\Uparrow|M_{1,x}|\Uparrow\rangle & \langle\Uparrow|M_{1,y}|\Uparrow\rangle & \langle\Uparrow|M_{1,z}|\Uparrow\rangle \end{bmatrix}, \quad (16)$$

where g depends on V_0 through the states $|\Uparrow\rangle, |\Downarrow\rangle$. The g-matrix can be factorized in the form (singular value decomposition) $g = U g_d V^T$, where U and V are 3×3 unitary matrices and $g_d = \mathrm{diag}(g_x, g_y, g_z)$ is a diagonal matrix, with g_x, g_y and g_z the principal g-factors.

By considering the derivative of g with respect to the gate voltage at $V_{\mathrm{CG}} = V_0$, $g'(V_0) = \left.\frac{\partial g(V_{\mathrm{CG}})}{\partial V_{\mathrm{CG}}}\right|_{V_{\mathrm{CG}}=V_0}$, one can express the Rabi frequency as

$$f_R = \frac{\mu_B B V_{ac}}{2h|g(V_0)\boldsymbol{b}|}\,|[g(V_0)\boldsymbol{b}] \times [g'(V_0)\boldsymbol{b}]|, \quad (17)$$

where $\boldsymbol{b} = \boldsymbol{B}/B$. The knowledge of $g(V_0)$ and $g'(V_0)$ is therefore sufficient to compute the Rabi frequency for any magnetic field direction. This procedure is correct to first order in $\boldsymbol{B}$ and V_{ac}.